Catena 162 (2018) 421–430

Contents lists available at ScienceDirect

Catena

journal homepage: www.elsevier.com/locate/catena

Sea level rise sedimentary record and organic carbon fluxes in a low-lying tropical coastal ecosystem

Vladislav Carnero-Bravo[a], Joan-Albert Sanchez-Cabeza[b,*], Ana Carolina Ruiz-Fernández[c], Martín Merino-Ibarra[d], José Antonio Corcho-Alvarado[e], Hans Sahli[e], Jean-François Hélie[f,g], Michel Preda[g], Jorge Zavala-Hidalgo[h], Misael Díaz-Asencio[i], Claude Hillaire-Marcel[f]

[a] Posgrado en Ciencias del Mar y Limnología, Universidad Nacional Autónoma de México, Ciudad Universitaria, 04510 Ciudad de México, Mexico
[b] Unidad Académica Procesos Oceánicos y Costeros, Instituto de Ciencias del Mar y Limnología, Universidad Nacional Autónoma de México, Ciudad Universitaria, 04510 Ciudad de México, Mexico
[c] Unidad Académica Mazatlán, Instituto de Ciencias del Mar y Limnología, Universidad Nacional Autónoma de México, Calz. Joel Montes Camarena s/n, 82040 Mazatlán, Sinaloa, Mexico
[d] Unidad Académica de Ecología y Biodiversidad Acuática, Instituto de Ciencias del Mar y Limnología, Universidad Nacional Autónoma de México, Ciudad Universitaria, 04510 Ciudad de Mexico, Mexico
[e] Spiez Laboratory, Federal Office for Civil Protection, CH-3700 Spiez, Switzerland
[f] Centre de Recherche sur la dynamique du système Terre (GEOTOP), Université du Québec à Montréal, 201 Avenue Président-Kennedy, Montréal H2X 3Y7, Canada
[g] Département des sciences de la Terre et de l'atmosphère, Université du Québec à Montréal, 201 Avenue Président-Kennedy, Montréal H2X 3Y7, Canada
[h] Centro de Ciencias de la Atmósfera, Universidad Nacional Autónoma de México, Ciudad Universitaria, 04510 Ciudad de México, Mexico
[i] Centro de Estudios Ambientales de Cienfuegos, AP5 Ciudad Nuclear, CP 59350 Cienfuegos, Cuba

ARTICLE INFO

Keywords:
Geochronology
Geochemistry
Sea-level
Carbon flux
Gulf of Mexico

ABSTRACT

Sea level rise, one of the most evident effects of recent climate change, is already impacting coastal ecosystems. Because of its low relief, population increase and economic development during the last century, the Celestun lagoon is highly vulnerable to global change, including sea level rise. Here, we study a sediment core from a tropical saltmarsh to evaluate the impact of sea level rise on sediment accretion and carbon fluxes. Some geochemical indicators in a ^{210}Pb dated sediment core showed clear signals of marine influence. This was reflected on increased accretion rates, from 0.3 ± 0.1 mm yr^{-1} in ≈1941 to 2.9 ± 1.2 mm yr^{-1} in 2012. These accretion rates were similar to eustatic sea level rise, and mean acceleration ranged from 0.037–0.22 mm yr^{-2}, implying a SLR by 2100 ranging from 14 to 86 cm. The one-century (1917–2013) organic carbon stock in sediments was calculated to be 10.1 ± 0.2 Mg C ha^{-1}. During the same period, the organic carbon flux, corrected for organic carbon degradation, increased from 7 ± 3 g C m^{-2} yr^{-1} to 73 ± 26 g C m^{-2} yr^{-1}, attributed to the impact of sea level rise in this ecosystem. This work shows that tropical saltmarshes may provide useful information on sea level rise, and the presented methodology may be used where instrumental records do not exist or they are too short.

1. Introduction

Sea level rise is threatening coastal ecosystems, reducing ecosystem services (e.g. storm protection, niche for species larval stage) and may, in the long term, cause profound socio-economic changes (SLR; Stocker et al., 2013). Low-lying coastal ecosystems are the most vulnerable ones to recent SLR. The Ría Celestún (Celestun coastal lagoon, Gulf of Mexico) is located in the northwestern Yucatan peninsula and encompasses a large diversity of ecosystems and species, some of which are endangered. It is inhabited by almost 7000 people, > 25% living in extreme poverty (SEDESOL, 2016). The main economic activities in the area are fishing, salt extraction and tourism (UNESCO, 2016). The maximum altitude of the Celestun Biosphere Reserve is only 3 m above local mean sea level, so it is highly vulnerable to SLR and extreme climatic events, such as tropical storms and hurricanes.

Although recent eustatic SLR, mainly caused by continental ice melting and seawater thermal expansion, is rather well known and thoroughly studied, specific ecosystem and socio-economic impacts will

* Corresponding author.
E-mail addresses: vladislavc@gmail.com (V. Carnero-Bravo), jasanchez@cmarl.unam.mx (J.-A. Sanchez-Cabeza), caro@ola.icmyl.unam.mx (A.C. Ruiz-Fernández), mmerino@cmarl.unam.mx (M. Merino-Ibarra), jose.corcho@babs.admin.ch (J.A. Corcho-Alvarado), hans.sahli@babs.admin.ch (H. Sahli), helie.jean-francois@uqam.ca (J.-F. Hélie), preda.michel@uqam.ca (M. Preda), jzavala@atmosfera.unam.mx (J. Zavala-Hidalgo), misaeldiazasencio1971@gmail.com (M. Díaz-Asencio), chm@uqam.ca (C. Hillaire-Marcel).

http://dx.doi.org/10.1016/j.catena.2017.09.016
Received 8 March 2017; Received in revised form 21 September 2017; Accepted 24 September 2017
Available online 03 November 2017
0341-8162/ © 2017 Elsevier B.V. All rights reserved.

be caused by local SLR, i.e. eustatic SLR corrected for vertical movements of the earth's crust and by long-term changes of atmospheric pressure, ocean currents and temperature (e.g. Nicholls and Cazenave, 2010; Wu et al., 2010).Therefore, in order to propose scientifically sound adaptation and mitigation strategies, long-term sea level time series are needed. However, for most of the world's coastal regions these are inexistent, too short or too sparse to obtain sound information. Near the Celestun coastal lagoon (90 km NE), the Servicio Mareográfico Nacional (Universidad Nacional Autónoma de México) manages a tide gauge in Progreso de Castro (Yucatan State), which has provided a rather continuous time series of tidal elevation during the period 1946–1985, partial records during 1994, and the continuous record was reestablished in 2012 (SMN, 2017). For the period 1953–1992, the estimated SLR rate in Progreso is 2.5 ± 1.2 mm yr^{-1} (Zavala-Hidalgo et al., 2010). Recently, eustatic SLR rate is estimated to be 2.8 ± 0.8 mm yr^{-1} during the period 1993–2009 (Church and White, 2011).

In the absence of long term tide gauge records, the only option to reconstruct the SLR trends within the past century may be ^{210}Pb dated sediment cores from coastal ecosystems, under the assumption that, to be preserved, the accretion rates in these environments are at least equivalent to the SLR elevation. Tropical saltmarshes (locally known as *marismas*) are usually found along semi-sheltered low-energy coastlines, protected from the open ocean, located behind the mangrove fringe in the highest topographic position within the tidal range, so they are intermittently inundated by medium to high tides. High evaporation and relatively infrequent flooding favor the formation of hypersaline soils that can be colonized by halophyte “glassworts”, vegetation (i.e. *Batis maritima* and *Salicornia pacifica*) that can tolerate inundation with seawater and high soil salinity (Costa et al., 2009; Ruiz-Fernández et al., 2016) or remain non-vegetated. When sediment supply is sufficient, saltmarshes are able to keep pace with SLR (Nolte et al., 2013), so the sedimentary record can provide useful information on local SLR (e.g. Lynch et al., 1989; Parkinson et al., 1994; Sanders et al., 2010a; Ruiz-Fernández et al., 2016).

In this work, we study the geochemical signals of SLR in a ^{210}Pb dated sediment core collected from a tropical saltmarsh in Celestun, a low-lying coastal lagoon in the southern Gulf of Mexico, and compare sediment accretion rates with eustatic SLR and with a nearby tide gauge station. It is expected that this information will help to better protect and plan sound adaptation and mitigation strategies for this important protected area.

2. Methods

2.1. Study site

The Yucatan Peninsula is a large karstic platform with mangrove forests and wetlands along its coastline. About 80% of the soils are shallow (leptosols; Bautista-Zúñiga et al., 2003) and lie on a highly permeable substrate, dominated by carbonates. Due to intense weathering, these soils are rich in insoluble oxides (Herbilion and Nahon, 1988).

The Celestun coastal lagoon (Fig. 1) is located on the northwestern side of the peninsula (20° 45′ N; 90° 23′ W). Ground water discharge to the lagoon induces a salinity and temperature gradient due to mixing with Gulf of Mexico seawater (Perry et al., 2009). The northern part of the Yucatan Peninsula is under a tropical wet/dry “AW” climate, according to the Köppen classification (Wilson, 1980). The mean annual rainfall is 760 mm, and climate shifts from warm medium-dry from March until May, to rainy from June to October, and to windy (strong winds locally known as “nortes”) from November to February. The Celestun coastal lagoon is narrow, approximately 22 km long and 2 km wide at its widest point. The vegetation is dominated by *Rhizophora mangle*, *Avicennia germinans* and *Laguncularia racemose* (Stalker et al., 2014).

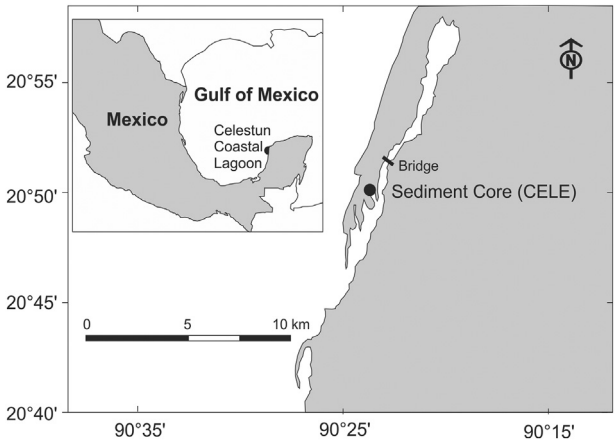

Fig. 1. Location of the Celestun coastal lagoon and location of the CELE sediment core.

The coastal plain in the Celestun region is bounded by the Ticul Fault, a karstic structure composed primarily of Early and Late Tertiary limestone platforms with a band of Quaternary beach and lagoon deposits (Pope et al., 1993). The aquifer is mostly unconfined, except near the coast where an impermeable caliche has formed near the fresh water discharge, which has migrated inland with rising Holocene sea level (Pope and Duller, 1989).

2.2. Sampling and analysis

Sampling was carried out in a non-vegetated area of a tropical saltmarsh, where a clear tidal influence was observed (Fig. 1). The sampling site height and location were measured with a Leica GS10 receiver and a Leica AS10 geodesic antenna, with a nominal vertical precision of 3.5 mm. Levelling was achieved with a Leica DNA03 digital level. The orthometric height was 0.302 m, i.e. close to the mean sea level.

The sediment core was collected on April 25th 2013 with a split push corer (PVC tube, inner diameter = 10 cm, length = 50 cm) and showed no compression. It was cut onsite into 1 cm sections, and samples were stored in air tight and acid cleaned plastic containers. Back to the laboratory, samples were freeze-dried. For grain size analysis (Table 1), samples were sieved through a 63 μm mesh, digested with 30% H_2O_2 and analyzed by laser diffraction with a Malvern Mastersizer 2000. The classifications reported were 0.1–2 μm (clay), 2–63 μm (silt) and 63–1000 μm (sand). Mineralogical analysis (halite and gypsum) was performed with a Siemens D5000 X-Ray diffractometer on a well-mixed sample.

Section aliquots were carefully ground with an agate mortar. Elemental composition was determined by X-ray fluorescence (XRF) spectrometry with a SPECTRO Xepos-3 system, calibrated with 34 reference materials. Analytical quality was monitored through the analysis of certified reference materials (IAEA-158 and PACS2). For OC analysis, inorganic carbon was removed by carefully adding by drops 5 mL of a HCl 1 N solution, which was left to react over two days. Acid was removed by diluting the sample to 40 mL with MilliQ water, centrifuged during 15 min at 3500 rpm, frozen for one day and freeze-dried for three days. The washing procedure was repeated until acid was fully removed. Organic carbon (OC) and total nitrogen (N) were determined with a CE Instruments Flash EA 1112 Element Analyzer and reported as % of the total dry weight. For quality assurance, the Calibration Sample (soil LECO Lot 10002, Part number 502-309) was measured every ten analyses. Recoveries (n = 12) were 102 ± 3% for N and 99 ± 1% for OC. δ^{13}C of organic matter was analyzed using an Elementar Vario Micro Cube™ elemental analyzer coupled to an Isoprime100™ isotope ratio mass spectrometer in continuous flow mode. The values are reported relative to VPDB (± 0.1‰ at 1σ) and the variation coefficient

Table 1
Basic statistics of all reported variables for sediment core CELE (Celestun coastal lagoon, Yucatan peninsula). Concentrations below the detection limit were not considered.

Variable	Unit	Minimum	Maximum	Mean	Analytical uncertainty %
Sand	%	46	95	87	3
Silt	%	3	48	9	7
Clay	%	2	8	3	8
Halite	%	1.7	9.8	3.5	–
Gypsum	%	0	14.1	2.8	–
Inorganic C (IC)	%	6.8	11.2	10.4	2
Organic C (OC)	%	0.42	4.35	0.96	11
N	%	0.033	0.626	0.081	9
C/N		7.5	10.8	9.2	5
Ca	%	4	29	22	1
Na	%	6	29	12	7
Cl	%	0.4	27.1	4.8	1
Mg	%	1.04	9.99	4.14	6
Si	%	0.02	3.76	1.57	2
S	%	0.28	1.81	0.46	2
Sr	%	0.10	0.21	0.18	1
K	%	0.06	0.32	0.11	2
Al	%	< 0.002	0.071	0.037	22
Fe	%	< 0.0001	0.025	0.011	3
Ti	%	0.004	0.014	0.007	4
P	$\mu g\ g^{-1}$	192	349	273	2
Br	$\mu g\ g^{-1}$	102	458	164	1
Mn	$\mu g\ g^{-1}$	12	28	21	5
Cr	$\mu g\ g^{-1}$	5	11	9	5
Ni	$\mu g\ g^{-1}$	5	13	6	7
Y	$\mu g\ g^{-1}$	< 0.5	4.7	3.4	7
Pb	$\mu g\ g^{-1}$	< 1.0	6.6	2.6	8
U	$\mu g\ g^{-1}$	< 1.0	5.0	1.7	16
$\delta^{13}C$	‰	− 21.31	− 15.50	− 19.50	0.1
^{210}Pb	$Bq\ kg^{-1}$	17	45	27	7
^{226}Ra	$Bq\ kg^{-1}$	22	30	26	8
^{239}Pu	$Bq\ kg^{-1}$	< 0.0009	0.0895	0.0528	2

was of 0.1‰ (replicate analysis of 3 samples).

The total OC sedimentary stock was obtained by integrating the OC contents of each dated section divided by the corer area (78.5 cm^2). To evaluate OC supply change with time, we multiplied OC concentrations by ^{210}Pb-derived MAR. Taking into consideration that buried OC is partially degraded, we reconstructed the OC concentrations that were deposited on the surface sediment layer before microbial decomposition, assuming steady-state diagenesis and that total organic carbon decomposes according to first-order kinetics (Middelburg, 1989; Ruiz-Fernández et al., 2011), by using the equation:

$$G_t = G_0 e^{-3.2\, t^{0.05}}$$

where G_t is the OC concentration at time t and G_0 is the OC concentration at the sediment surface. With the asymptotic value downcore, we reconstructed the theoretical decay fractions per section, which were then used to reconstruct the original OC concentration profile and flux evolution. The OC decomposition half-life was calculated by using the first-order G-model (Berner, 1980; Zimmerman and Canuel, 2000).

For radiochronology, ^{210}Pb activities were determined through the analysis of its radioactive descendent ^{210}Po by alpha spectrometry, assuming secular equilibrium between both radionuclides, following the method described by Ruiz-Fernández et al. (2009). Briefly, sediment aliquots (≈ 0.25 g) were spiked with the yield tracer ^{209}Po and were totally digested with a mixture of acids (1:5:4 HF + HNO_3 + HCl) in closed PFA containers overnight at 120 °C. The solution was fully evaporated, the residue was rinsed with concentrated HCl, evaporated several times and finally dissolved in 0.5 M HCl in presence of ascorbic acid. Po isotopes were spontaneously deposited on an Ag disc and their activities were measured by alpha spectrometry (Ortec-Ametek).

Gamma emitters were measured by high-resolution gamma spectrometry using a high purity germanium detector with well configuration (ORTEC GWL-120-15-S). Efficiency calibration for energies of interest was performed with the Standard Uranium Ore (IAEA-RGU-1) and a Certified Reference Solution QCY44 (Amersham). Sample specific efficiency correction was performed with ANGLE (ORTEC). For quality assurance, the materials IAEA-313 (Stream sediment), IAEA-385 (Irish Sea sediment) and IAEA-384 (Fangataufa sediment) were analyzed. All measurements were within the certified values (2 sigma). Samples were placed into calibrated geometries (4 mL), stored for at least 3 weeks, counted for several days and ^{226}Ra determined via the 352 keV gamma rays emitted by its daughter radionuclide ^{214}Pb.

Sediment core chronology, including mass accumulation rates (MAR) and sediment accumulation rates (SAR), was obtained by using the Constant Flux (CF) model (Robbins, 1978; Sanchez-Cabeza and Ruiz-Fernández, 2012), also known as the Constant Rate of Supply (CRS) model (Appleby and Oldfield, 1978), as this model allows to calculate chronologies and accumulation rates when these are not constant. This is expected as the Yucatan peninsula is on a karstic platform, with water table fluctuation and biological productivity variability. Uncertainties were estimated with a Monte Carlo method (Sanchez-Cabeza et al., 2014). The CF model is commonly used in coastal ecosystems as it accounts for variable accumulation rates (e.g. Appleby and Oldfield, 1983; Roman et al., 1997; Lubis, 2013; Cuellar-Martinez et al., 2017) by assuming a constant flux of $^{210}Pb_{ex}$ to the sediment surface. As the chronology is only dependent on the total $^{210}Pb_{ex}$ activity for each section, it is also independent of compaction and matrix change effects.

^{239}Pu was determined by mass spectrometry and used to validate the chronology. Samples were dissolved by fusion and purification was performed with TEVA (Triskem International) resins (Röllin et al., 2009). Measurement was performed with a Neptune plus high resolution double focusing multicollector ICP-MS (Thermo Scientific Inc.) equipped with ten Faraday collectors and five ion counters. Aqueous solutions were introduced into the ICP-MS using a CETAC Arridus II desolvator (Elemental Scientific Inc.). Quality was assured by analyzing the certified reference materials IAEA-327, IAEA-384 and IAEA-447. All measurements were close to the certified value.

2.3. Geochemical characterization

Geochemical and stratigraphic variables are useful for the interpretation of processes recorded in the sedimentary profile. Grain size might affect elemental composition and/or organic carbon concentration. $\delta^{13}C$ is a reliable tracer of organic carbon sources, and marine sources (such as phytoplankton and seagrasses) are characterized by $\delta^{13}C$ values within the range − 23 to − 17‰ (Kristensen et al., 2008). Al and Ti are conservative elements often used as tracers of terrigenous material inputs (Loring and Rantala, 1992; Nesbitt and Markovics, 1997). Fe and Mn enter the marine environment due to weathering of continental silicate rocks, and can be used to identify the environmental redox conditions in the sedimentary column (Cochran et al., 1998). The C/N ratio can be used to identify the source of organic matter (supporting/complementing $\delta^{13}C$; Meyers, 1994). Na, Cl and Br are typical elements of marine inputs (Wedepohl, 1971) and their profile behavior can be helpful to infer marine influence (Ruiz-Fernández et al., 2016).

Principal component analysis (PCA) allows to evaluate the association of variables with extracted components through their loadings (ranging from − 1 to 1). The relevance of each component is assessed though its explained variance. Profile shape inspections and PCA results provide useful information to infer possible environmental processes.

3. Results

Concentrations, activities, ranges and means of all measurements are shown in Tables 1 and S1 (Supporting information). The levels of

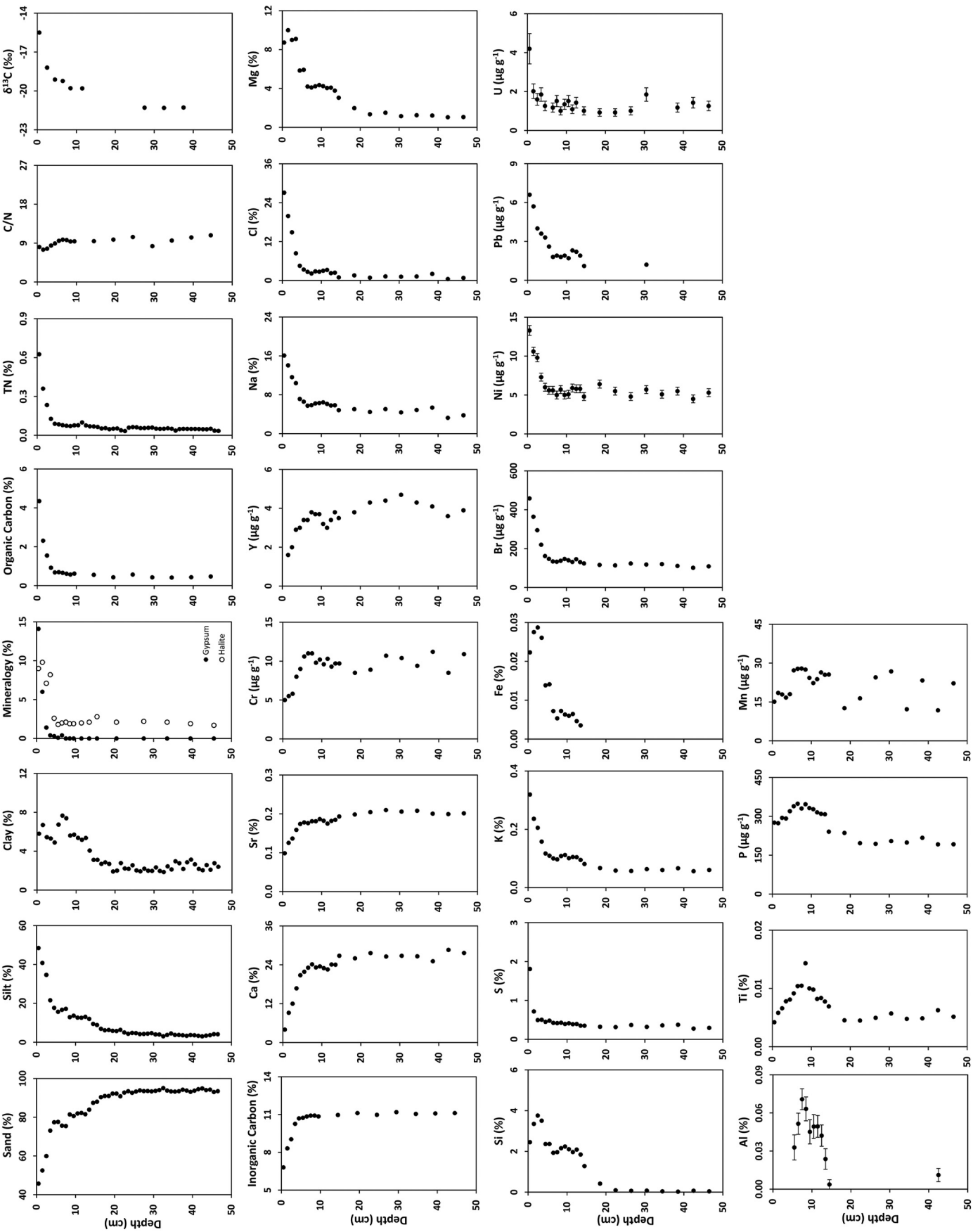

Fig. 2. Depth profiles of all variables measured for core CELE, Yucatan. Mexico.

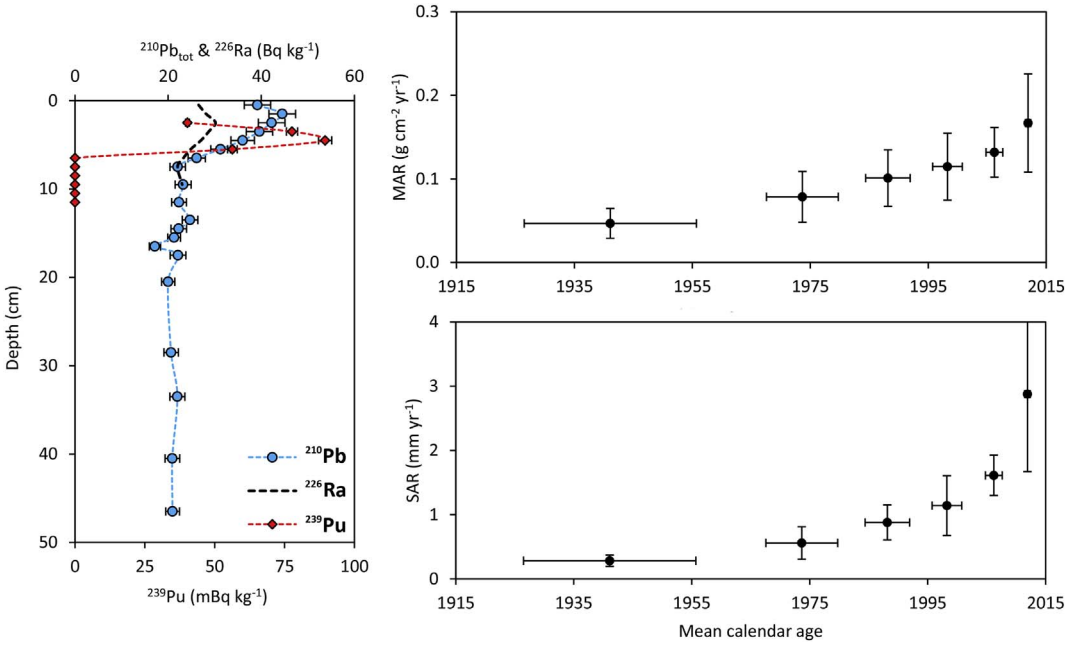

Fig. 3. ^{210}Pb sediment dating results in core CELE, Yucatan, Mexico: a) ^{210}Pb and ^{239}Pu concentration profiles (left), b) mass accumulation rates (MAR; right up), and c) sediment accumulation rates (SAR; right down).

some variables, which are usually related to terrestrial input from aluminosilicate environments, were very low (i.e. nitrogen, Ti, Al, P, Y, Cr and Mn), or even below detection limits (magnetic susceptibility, not reported) because of the carbonate nature of the Yucatan peninsula.

Based on the concentration profiles, three groups of variables were identified. The first group (Fig. 2: Na, Si, Cl, Mg, K, Fe, Ni, Br, Pb, δ^{13}C, organic C, total N, silt, halite and gypsum) showed an increase toward the surface, while a second group (Fig. 2: sand, inorganic C, Ca, Sr, Cr and Y) showed the opposite trend. The third group showed profiles with a sub-surface peak (Fig. 2: Ti, Al, P and clays), although they presented low concentration values. In all cases, all variables showed almost constant concentrations below 20 cm, some of them even below 6–10 cm (gypsum, halite, OC, TN, IC, Cr, S, Ni and U).

Total ^{210}Pb activities ranged from 17 ± 1 to 45 ± 3 Bq kg^{-1} (Fig. 3). The profile showed a constant total ^{210}Pb concentration below 7 cm, equivalent to ^{226}Ra activities in sections 7–8 and 9–10 cm (Fig. 3). The core chronology is showed in Table S1 (Supplementary information). The oldest datable section (5–6 cm) showed a mean age of 1941 (range 1917–1966). Although it is common to use ^{137}Cs for chronology validation by observing its expected maximum in 1963, activities were below the detection limit (1–2 Bq kg^{-1}), which is also the case in other Mexican coastal areas, due to its low atmospheric flux in the region, radioactive decay since global fallout and ^{137}Cs solubility in sea water (Ruiz-Fernández and Hillaire-Marcel, 2009; Cuellar-Martinez et al., 2017).

The ^{239}Pu profile showed a clear maximum in section 4–5 cm, corresponding to the time interval 1966 ± 10–1982 ± 6. The lower age of the section is, within the age uncertainties, consistent with the expected maximum tropospheric concentration of man-made radionuclides in 1962–64. The apparent time delay observed (≈ 2 yr) in the ^{239}Pu maximum might also be due to the long time residence of plutonium in surface ocean (Hirose et al., 2007) and coastal (Corcho-Alvarado et al., 2014) waters, which would cause a delay in the signal recorded in sediments. Both MAR and SAR showed similar time trends, increasing from minimum values in the older section to higher values in the surface. In the case of SAR, the trend increased from 0.24 ± 0.09 mm yr^{-1} in the oldest section (mean age 1941) to 3.6 ± 1.2 mm yr^{-1} in the surface section (mean age 2012).

4. Discussion

Eustatic SLR is one of the main manifestations of recent climate change, and local SLR is responsible for important impacts on coastal ecosystems. Because of its low elevation and slope, the Celestun lagoon area is especially vulnerable to sea level rise. Marine transgression may affect coastal infrastructures and services, including springs and freshwater supply (Nicholls and Cazenave, 2010). In addition, mangroves are threatened because of increasing salinities due to longer inundation periods and, particularly in the case of the Yucatan peninsula, lack of sediment supply due to the absence of rivers, thus compromising the ability of the ecosystem to keep pace with SLR (McKee et al., 2007; McKee, 2011).

4.1. Geochemical signature of sea level rise

The CELE core, located near the tide high tide mark between the lagoon's mouth and the middle part, showed a high sand percentage along most of the record (> 90%), and a progressive increase of silts from 17 cm upwards (from 9 to 48%). The grain size transition was outside the ^{210}Pb dating temporal range and no clear attribution can be made. We speculate that this transition may be a consequence of the establishment of modern population in Celestún, around 1718 (SEFOE, 2017). The grain size change could be related to the supply of finer sediments transported from the catchment, as result of agricultural development. The core also showed an important sand fraction reduction above 5 cm (≈ 1966) and an increase of marine proxies (e.g. Br, Cl and Na, Fig. 2), probably resulting from changes in water circulation and infilling, associated to the construction of a bridge across Celestun Lagoon around 1963 (Gonneea et al., 2004). The agreement between the observed recent geochemical changes and the bridge construction within the same period, may be considered as a further validation of the ^{210}Pb derived chronology.

In order to identify underlying environmental processes, we performed a factor analysis (FA) with principal components analysis (PCA) extraction with all variables except those used for or derived from radiochronology (^{210}Pb, ^{226}Ra, ^{239}Pu, SAR and MAR). The PCA

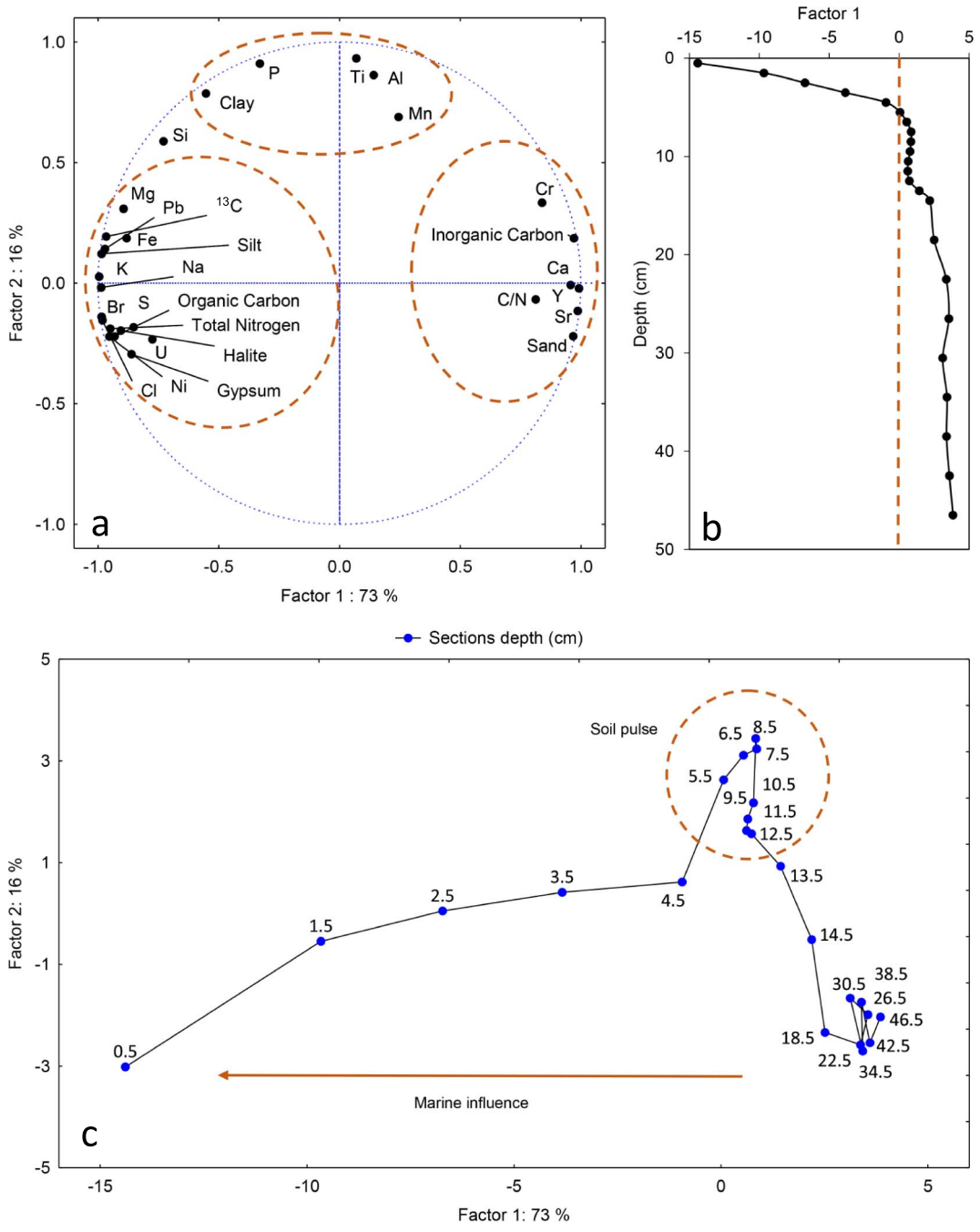

Fig. 4. Factor analysis with Principal Components extraction of all variables, except those used for or derived from radiochronology.

extracted two factors that explained 89% of the data base variance. Factor one (73% of explained variance) included, with significative negative loadings, Na, Cl and Br, typical marine proxies (Wedepohl, 1971). This was confirmed by the strong negative loadings of $\delta^{13}C$ (Fig. 4a), a good indicator of marine conditions (Kristensen et al., 2008), and also observed in similar environments (Carnero-Bravo et al., 2016; Ruiz-Fernández et al., 2016). In core CELE, $\delta^{13}C$ ranged from -21.3 to -15.5‰, and C/N ranged from 7 to 12, indicating the presence of marine OC along the core, and an upward trend of increasing marine conditions. A similar observation was made in a sediment core near the Celestun lagoon mouth, attributed to a shift from mangrove-dominated to seagrass-dominated organic matter (Gonneea et al., 2004). Positive loadings are observed for Ca, Sr and inorganic carbon. Bearing in mind that the Yucatan peninsula has a carbonaceous origin, these variables were attributed to a continental origin. In summary, Factor 1 is negative for marine conditions, and positive for continental conditions.

Factor 1 (Fig. 4b) shows positive (i.e. continental) values from the core bottom up to 5 cm (1966 ± 10). From then onwards, a steady progression to very negative values (i.e. marine) was observed. In agreement with a similar observation in tropical saltmarshes in the NE Pacific coast, we refer to this factor as *Marine influence* (Ruiz-Fernández et al., 2016). This factor indicates that since 1966 the site is subject to an increasingly larger marine influence due to local SLR. In this zone, marine conditions recorded in sediments are characterized by an enrichment in silt, organic matter, halite, gypsum, Na, Cl and Br, which show maximum concentrations at the core surface (Fig. 2).

The concentrations typical terrigenous proxies in alumino-silicate environments (notably Al and Ti), were very low, as expected for a carbonate platform. Nevertheless, the Al and Ti depth profiles showed a

Table 2
Organic carbon fluxes in mangrove ecosystems.

Study area	Organic carbon flux[a] ($g\ m^{-2}\ yr^{-1}$)			Period	Reference
	Mean	Min.	Max.		
Worldwide reviews					
Different types of mangrove ecosystems	100				Twilley et al. (1992)
Globally averaged	210 (20)				Chmura et al. (2003)[c]
Geometric mean of published reports	139 (24)				Duarte et al. (2005)
Mangroves	226 (39)	20	949		Mcleod et al. (2011)
Confidence interval (95%) for the geometric mean	163 (+ 40) (− 31)				Breithaupt et al. (2012)
Riverine presence					
Cananéia (Ribeira of Iguape River), Brazil	192				Sanders et al. (2010b)
Tamandaré (Formoso River), Brazil	353				Sanders et al. (2010b)
Everglades National Park (Shark River), Florida, USA	139			1924–2000	Smoak et al. (2013)
Everglades National Park (Shark River), Florida, USA	144			1926–2000	Smoak et al. (2013)
Everglades National Park (Shark River), Florida, USA	260			2000–2009	Smoak et al. (2013)
Everglades National Park (Shark River), Florida, USA	393			2000–2009	Smoak et al. (2013)
Everglades National Park (Shark River), Florida, USA	225 (61)			2000–2010	Breithaupt et al. (2014)
Everglades National Park (Shark River), Florida, USA	176 (31)			1960–2010	Breithaupt et al. (2014)
Everglades National Park (Shark River), Florida, USA	123 (19)			1910–2010	Breithaupt et al. (2014)
Moreton Bay (Brisbane, Logan and Caboolture rivers), Australia	150			1920–2000	Sanders et al. (2016)
Moreton Bay (Brisbane, Logan and Caboolture rivers), Australia	1000			2000–2013	Sanders et al. (2016)
Rookery Bay (Henderson Creek), Florida, USA		222 (39)	381 (23)		Cahoon and Lynch (1997)[b]
Rookery Bay (Henderson Creek), Florida, USA		69	99		Breithaupt et al. (2012)
Soledad Lagoon (Sinu River), Colombia		314	409		Ruiz-Fernández et al. (2011)
Hinchinbrook Channel (Herbert River), Australia		26	336		Breithaupt et al. (2012)
Matang Reserve (numerous rivers), Malaysia		148	410		Breithaupt et al. (2012)
Jiulongjiang Estuary (Jiulongjiang River), China		168	840		Alongi et al. (2005)
Fukido (small river), Ishigaki, Japan		22	230		Tateda et al. (2005)
DaLoc (high river discharge), ThanHoa, Vietnam		120	180		Tateda et al. (2005)
Trat (high river discharge), Thailand		100	600		Tateda et al. (2005)
Sawi Bay (Khlong Sawi & Khlong I Laet), Thailand		184	281		Breithaupt et al. (2012)
Irian Jaya (Ajkwa River), Indonesia		412	717		Breithaupt et al. (2012)
Boca Chica (Palizada River), Terminos Lagoon, Mexico		79	237		Breithaupt et al. (2012)
Limited river-influence					
Ilha Grande, Brazil	186				Sanders et al. (2010b)
Terminos Lagoon, Mexico		53	65		Gonneea et al. (2004)
Estero Pargo, Terminos Lagoon, Mexico		75	157		Breithaupt et al. (2012)
Limited surface run-off (karstic environments)					
Chelem Lagoon, Mexico		67	104		Gonneea et al. (2004)
Celestun Lagoon, Mexico		55	70		Gonneea et al. (2004)
Celestun Lagoon, Mexico	*11 (4)*	*7 (3)*	*15 (5)*	*1917–1995*	*This work*
Celestun Lagoon, Mexico	*47 (19)*	*27 (9)*	*73 (26)*	*1995–2013*	*This work*

[a] Reported uncertainties in brackets.
[b] Originally reported as organic matter (transformation factor used: 0.58).
[c] Re-evaluation made by Breithaupt et al. (2012).

similar subsurface peak before 1916 (Fig. 2), and maxima were also observed for clay content, Mn and P concentrations. Although the presence of a Mn peak may sometimes be attributed to a change in redox conditions (the so-called redox front), its close association with Ti and Al, and no other redox sensitive elements, suggests that Mn also has, in this case, a continental origin.

Factor 2 (16% explained variance) has significant positive loadings with these elements (Ti, Al, Mn), with clays and P (Fig. 4), but no variables showed negative loadings, suggesting that this is not a two end-member process. In tropical regions, intense rainfall causes mineral leaching, thus leaving behind calcite and other insoluble oxides, such as Al and Ti (Herbilion and Nahon, 1988). In the Yucatan peninsula, Al oxide in leptosols range from 20 to 27% (Bautista-Zúñiga et al., 2003). We therefore referred to this factor as *Soil pulse*. Although this pulse occurs beyond the ^{210}Pb dating range, it likely occurred during the XIX century, and we speculate that Al-rich fine particle soils from the catchment reached the site due to strong meteorological events, such as heavy rains that could have transported fine particles with runoff. As a matter of fact, NOAA reports four tropical depressions and storms directly hitting the Celestun lagoon in the period 1851–1900 (NOAA, 2016).

4.2. Sediment accumulation and sea level rise

Both sediment (SAR) and mass (MAR) accumulation rates exhibited the same steady increase since the 1940s to the present (Fig. 3), in keeping with the increasing marine conditions. Hydrodynamic changes in this lagoon are dominated by wind and freshwater discharge (Casares-Salazar and Mariño-Tapia, 2016). The annual and sub-annual frequency of these events cannot be resolved in our sedimentary record, nor may likely affect the observed SAR and MAR long-term trend of about 80 years.

Maximum SAR and MAR occur in the uppermost section (2011 − 2013) with values of 2.9 ± 1.2 mm yr^{-1} and 0.17 ± 0.06 g $cm^{-2}\ yr^{-1}$ respectively. In Belize (Caribbean Sea), SAR in the mangrove fringe zone ranged from 1.2 to 2.8 mm yr^{-1} (McKee et al., 2007; McKee, 2011). In the Sian Ka'an Biosphere Reserve (eastern Yucatan Peninsula) in a tropical saltmarsh, SAR increased from 1.2 ± 0.3 mm yr^{-1} (1950–1985) to 3.1 ± 0.9 mm yr^{-1} (1985–2013) (Carnero-Bravo et al., 2016). The maximum SAR in Celestun is remarkably similar to the eustatic SLR during 1993–2009 of 2.8 ± 0.8 mm yr^{-1} (Church and White, 2011), indicating that SAR

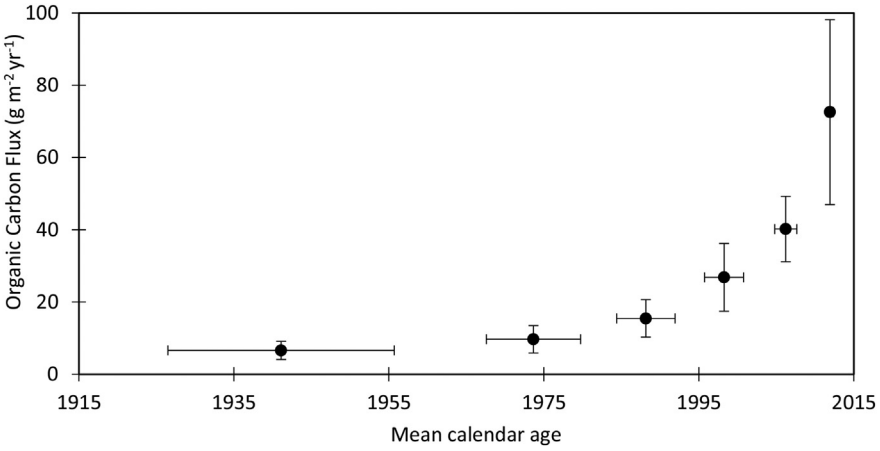

Fig. 5. Organic carbon fluxes in sediment core CELE, Yucatan, Mexico. Fluxes were corrected following Middelburg (1989).

observed in cores collected from the high tide mark in tropical saltmarshes may provide reliable information on SLR and allow the reconstruction of local SLR. We also suggest that the observed increase of marine conditions, derived from geochemical information, is in fact due to SLR. Assuming a SLR value of 3 mm yr^{-1}, and a ^{210}Pb seawater concentration of circa 1 Bq m^{-3} (e.g. Masqué et al., 2002), the increased seawater ^{210}Pb inventory due to SLR is only of 0.003 Bq m^{-2} yr^{-1}, i.e. < 0.01% of the ^{210}Pb atmospheric flux (mean of the values reported by Carnero-Bravo et al., 2016). Therefore, we concluded ^{210}Pb chronologies of tropical saltmarshes are unaffected by present SLR.

Assuming that, in this area, local SLR is similar to the calculated SAR in core CELE, we inferred that sea level has been increasing since the sedimentary record started (1917). We derived the SLR rate (i.e. acceleration) between two sections by diving the SAR increase by the time lapse between them. The acceleration was estimated as i) 0.037 mm yr^{-2}, when considering the full record (i.e. since 1941), and ii) 0.22 mm yr^{-2}, when considering only the first to sections (i.e. since 2006). Taking the conservative assumption that the acceleration will be constant until 2100, the local mean sea level above its present value would range from 14 to 86 cm.

4.3. Organic carbon flux

Mangrove ecosystems are known to have a high carbon sequestration potential (Chmura et al., 2003). Once buried, OC degrades mainly through bacterial mineralization, usually following an exponential decay (Berner, 1980), similar to the observed OC depth profile at Celestun (Fig. 2). We defined excess OC as section OC minus the value in section 5–6 (the oldest datable section). In the case of core CELE, both the correlation and linear regression of ln (excess OC) versus mean deposition time are highly significative (R^2 = 0.99, $p \ll 0.05$), thus confirming that the empirical and steady-state Middelburg (1989) model can be used.

Mangrove forests are present in very diverse environments, and the reported worldwide mean OC flux in mangrove areas is 163 (+ 40) (− 30) g m^{-2} yr^{-1} (Breithaupt et al., 2012). The largest OC fluxes are observed in river dominated mangrove forests (Table 2), ranging from a minimum of 22 g m^{-2} yr^{-1} in Fukido, Ishigaki, Japan (Tateda et al., 2005), to values as high as 840 g m^{-2} yr^{-1} in the Jiulongjiang Estuary, China, which is a highly eutrophic ecosystem (Alongi et al., 2005) and 1023 g m^{-2} yr^{-1} in an impacted mangrove in Cubatão, Brazil (Sanders et al., 2014). In ecosystems with low riverine influence, the OC flux range is apparently smaller, ranging from 53 g m^{-2} yr^{-1} in Terminos lagoon (Gonneea et al., 2004) to 186 g m^{-2} yr^{-1} in Ilha Grande, Brazil (Sanders et al., 2010b), and also low in areas with limited surface runoff (e.g. 104 g m^{-2} yr^{-1} in Chelem lagoon, Mexico; Gonneea et al., 2004).

The OC contents in core CELE decreased from a surface value of 4.35 ± 0.23% to a mean value of 0.51 ± 0.08% below 6 cm, and we calculated an apparent half-life of 15 yr. The total OC stock in the sediment core during the dated time rage (1917–2013, almost one century) was 10.1 ± 0.2 Mg C ha^{-1}. The original OC flux along the core (Fig. 5) was estimated with a model of organic matter degradation (Middelburg, 1989) to the mean age of the uppermost section. The original OC fluxes in the CELE core ranged from 7 ± 3 g m^{-2} yr^{-1} (1941) to a present (2013) value of 73 ± 26 g m^{-2} yr^{-1}. These values are relatively low when compared with worldwide mangrove studies (Table 2), and the OC flux increase might be due to a hydrological change from a higher to a lower energy environment, then accumulating finer (organic rich) particles. The synchronous increasing trends of OC flux and marine indicator elements since the 1940s suggested that, locally, SLR changed the lagoon hydrodynamics and, in turn, strengthens marine OC sequestration capacity in this tropical saltmarsh area. If this observation was confirmed in other tropical saltmarshes worldwide, this might have important implications in the calculation of marine carbon stocks (the so-called blue carbon, Mcleod et al., 2011) and climate modelling, as this might imply a climate feedback mechanism.

5. Conclusions

The geochemical signatures in a sediment core from a tropical saltmarsh from the Celestun coastal lagoon in the Yucatan Peninsula (Gulf of Mexico) indicated increasing marine conditions since 1966 ± 10, which we attributed to an increase in flooding in this site. The increasing marine conditions were characterized by an increase of, amongst other tracers, Na, Cl, Br, halite, gypsum and silt, and a decrease of Ca, Sr and sand. A small subsurface peak of Al and Ti was attributed to a process that transported fine soil particles to the area. ^{210}Pb derived sediment accumulation rates (SAR) showed a progressive increase from 0.3 ± 0.1 mm yr^{-1} in 1941 to 2.9 ± 1.2 mm yr^{-1} at the core surface (2012). The recent value is similar to the eustatic SLR observed during 1993–2009, suggesting that i) tropical saltmarshes can keep pace with sea level rise, ii) cores in these environments can provide reliable reconstructions of SLR (100 yr), and iii) the peninsula shows little, if any, vertical movement, confirming the usefulness of these region to study the global impact of sea level rise. During the full time record (since 1941), the estimated acceleration was 0.037 mm yr^{-2}, implying a SLR of 14 cm by the end of the XXI century. However, when considering only the first 2 sections (since 2006), the estimated acceleration was 0.22 mm yr^{-2}, suggesting a maximum SLR of 86 cm by 2100, assuming that it remains constant.

The original (degradation corrected) organic carbon flux increased tenfold, from 7 ± 3 in 1941 to 73 ± 26 g m^{-2} yr^{-1} at present. This marine OC increase was attributed to SLR and, if confirmed in other

environments, this might have important implications for the calculation of marine carbon stocks (blue carbon) and climate modelling, as this would be a feedback mechanism. This work shows that tropical saltmarshes may preserve several signatures of sea level rise, and that this methodology may be used where tide-gauge records do not exist or are too short. This information is crucial for proper planning of coastal zone development, and to plan adaptation and mitigation strategies to climate change impacts, including those caused by sea level rise.

Acknowledgements

The study was funded through research grants CONACyT CB2010-153492, PDCPN2013-01/214349, PDCPN-2015-1-473 and bilateral Mexico-Quebec C0005-2013-01/0196813, PAPIIT-IN203313, PRODEP, and a CONACYT fellowship to VCB. Eduardo Batllori (Secretaría de Desarrollo Urbano y Medio Ambiente, SEDUMA) proposed sampling sites. Jorge Novelo and Jorge Luís Serrato de la Peña (UNAM) provided support for sampling. High-quality topography was performed by José Antonio Santiago Santiago, Felipe Hernández Maguey and Sergio Valente Gutiérrez Quijada (Servicio Mareográfico Nacional, Instituto de Geofísica, UNAM). Laboratory support was provided by Libia Hascibe Pérez Bernal (laboratory analysis), Agnieszka Adamowicz-Walczak (GEOTOP, UQAM, mass spectrometry), and Stefan Röllin (Spiez Laboratory, MC-ICP-MS). Maps were prepared by Germán Ramírez Reséndiz and Carlos Suárez Gutiérrez.

Appendix A. Supplementary data

Supplementary data associated with this article can be found in the online version, at https://doi.org/10.1016/j.catena.2017.09.016. These data include the Google map of the most important areas described in this article.

References

Alongi, D.M., Pfitzner, J., Trott, L.A., Tirendi, F., Dixon, P., Klumpp, D.W., 2005. Rapid sediment accumulation and microbial mineralization in forests of the mangrove *Kandelia candel* in the Jiulongjiang Estuary, China. Estuar. Coast. Shelf Sci. 63 (4), 605–618.

Appleby, P.G., Oldfield, F., 1978. The calculation of lead-210 dates assuming a constant rate of supply of unsupported ^{210}Pb to the sediment. Catena 5 (1), 1–8.

Appleby, P.G., Oldfield, F., 1983. The assessment of ^{210}Pb data from sites with varying sediment accumulation rates. Hydrobiologia 103 (1), 29–35.

Bautista-Zúñiga, F., Jiménez-Osornio, J., Navarro-Alberto, J., Manu, A., Lozano, R., 2003. Microrelieve y color del suelo como propiedades de diagnóstico en Leptosoles cársticos. Terrain 21 (1), 1–11.

Berner, R.A., 1980. Early Diagenesis, A Theoretical Approach. Princeton University Press, Princeton, N.J., pp. 241.

Breithaupt, J.L., Smoak, J.M., Smith, T.J., Sanders, C.J., Hoare, A., 2012. Organic carbon burial rates in mangrove sediments: strengthening the global budget. Glob. Biogeochem. Cycles 26 (3).

Breithaupt, J.L., Smoak, J.M., Smith, T.J., Sanders, C.J., 2014. Temporal variability of carbon and nutrient burial, sediment accretion, and mass accumulation over the past century in a carbonate platform mangrove forest of the Florida Everglades. J. Geophys. Res. Biogeosci. 119 (10), 2032–2048.

Cahoon, D.R., Lynch, J.C., 1997. Vertical accretion and shallow subsidence in a mangrove forest of southwestern Florida, USA. Mangrove Salt Marshes 1 (3), 173–186.

Carnero-Bravo, V., Sanchez-Cabeza, J.A., Ruiz-Fernández, A.C., Merino-Ibarra, M., Hillaire-Marcel, C., Corcho-Alvarado, J.A., Rölling, S., Diaz-Asencio, M., Cardoso-Mohedano, J.G., Zavala-Hidalgo, J., 2016. Sedimentary records of recent sea level rise and acceleration in the Yucatan Peninsula. Sci. Total Environ. 573, 1063–1069.

Casares-Salazar, R., Mariño-Tapia, I., 2016. Influence of the remote forcing and local winds on the barotropic hydrodynamics of an elongated coastal lagoon. J. Coast. Res. 32 (1), 116–130.

Chmura, G.L., Anisfeld, S.C., Cahoon, D.R., Lynch, J.C., 2003. Global carbon sequestration in tidal, saline wetland soils. Glob. Biogeochem. Cycles 17 (4).

Church, J.A., White, N.J., 2011. Sea-level rise from the late 19th to the early 21st century. Surv. Geophys. 32 (4–5), 585–602.

Cochran, J.K., Frignani, M., Salamanca, M., Bellucci, L.G., Guerzoni, S., 1998. Lead-210 as a tracer of atmospheric input of heavy metals in the northern Venice Lagoon. Mar. Chem. 62 (1), 15–29.

Corcho-Alvarado, J.A., Diaz-Asencio, M., Froidevaux, P., Bochud, F., Alonso-Hernández, C.M., Sanchez-Cabeza, J.A., 2014. Dating young Holocene coastal sediments in tropical regions: use of fallout ^{239,240}Pu as alternative chronostratigraphic marker. Quat. Geochronol. 22, 1–10.

Costa, C.S.B., Iribarne, O.O., Farina, J.M., 2009. Human impacts and threats to the conservation of South American salt marshes. In: Silliman, B.R., Grosholz, E.D., Bertness, M.D. (Eds.), Human Impacts on Salt Marshes: A Global Perspective. University of California Press, Berkeley, CA, pp. 337–360.

Cuellar-Martinez, T., Ruiz-Fernández, A.C., Sanchez-Cabeza, J.A., Alonso-Rodríguez, R., 2017. Sedimentary record of recent climate impacts on an insular coastal lagoon in the Gulf of California. Quat. Sci. Rev. 160, 138–149.

Duarte, C.M., Middelburg, J.J., Caraco, N., 2005. Major role of marine vegetation on the oceanic carbon cycle. Biogeosciences 2 (1), 1–8.

Gonneea, M.E., Paytan, A., Herrera-Silveira, J.A., 2004. Tracing organic matter sources and carbon burial in mangrove sediments over the past 160 years. Estuar. Coast. Shelf Sci. 61 (2), 211–227.

Herbilion, A.J., Nahon, D., 1988. Laterites and laterization processes. In: Iron in Soils and Clay Minerals. Springer Netherlands, pp. 779–796.

Hirose, K., Aoyama, M., Fukasawa, M., Kim, C.S., Komura, K., Povinec, P.P., Sanchez-Cabeza, J.A., 2007. Plutonium and ^{137}Cs in surface water of the South Pacific Ocean. Sci. Total Environ. 381 (1), 243–255.

Kristensen, E., Bouillon, S., Dittmar, T., Marchand, C., 2008. Organic carbon dynamics in mangrove ecosystems: a review. Aquat. Bot. 89 (2), 201–219.

Loring, D.H., Rantala, R.T.T., 1992. Geochemical analyses of marine sediments and suspended particulate matter. Fisheries and Marine Services 58 Technical Report 700.

Lubis, A.A., 2013. Constant rate of supply (CRS) model for determining the sediment accumulation rates in the coastal area using ^{210}Pb. J. Coast. Dev. 10 (1), 9–18.

Lynch, J.C., Meriwether, J.R., McKee, B.A., Vera-Herrera, F., Twilley, R.R., 1989. Recent accretion in mangrove ecosystems based on ^{137}Cs and ^{210}Pb. Estuaries 12 (4), 284–299.

Masqué, P., Sanchez-Cabeza, J.A., Bruach, J.M., Palacios, E., Canals, M., 2002. Balance and residence times of ^{210}Pb and ^{210}Po in surface waters of the northwestern Mediterranean Sea. Cont. Shelf Res. 22 (15), 2127–2146.

McKee, K.L., 2011. Biophysical controls on accretion and elevation change in Caribbean mangrove ecosystems. Estuar. Coast. Shelf Sci. 91 (4), 475–483.

McKee, K.L., Cahoon, D.R., Feller, I.C., 2007. Caribbean mangroves adjust to rising sea level through biotic controls on change in soil elevation. Glob. Ecol. Biogeogr. 16 (5), 545–556.

Mcleod, E., Chmura, G.L., Bouillon, S., Salm, R., Björk, M., Duarte, C.M., Lovelock, C.E., Schlesinger, W.H., Silliman, B.R., 2011. A blueprint for blue carbon: toward an improved understanding of the role of vegetated coastal habitats in sequestering CO_2. Front. Ecol. Environ. 9 (10), 552–560.

Meyers, P.A., 1994. Preservation of elemental and isotopic source identification of sedimentary organic matter. Chem. Geol. 114 (3–4), 289–302.

Middelburg, J.J., 1989. A simple rate model for organic matter decomposition in marine sediments. Geochim. Cosmochim. Acta 53 (7), 1577–1581.

Nesbitt, H.W., Markovics, G., 1997. Weathering of grandioritic crust, long-term storage of elements in weathering profiles, and petrogenesis of siliciclastic sediments. Geochim. Cosmochim. Acta 61 (8), 1653–1670.

Nicholls, R.J., Cazenave, A., 2010. Sea-level rise and its impact on coastal zones. Science 328 (5985), 1517–1520.

NOAA (National Oceanic and Atmospheric Adiministration), 2016. https://coast.noaa.gov/hurricanes/ (consulted on 2016/09/16).

Nolte, S., Koppenaal, E.C., Esselink, P., Dijkema, K.S., Schuerch, M., De Groot, A.V., Bakker, J.P., Temmerman, S., 2013. Measuring sedimentation in tidal marshes: a review on methods and their applicability in biogeomorphological studies. J. Coast. Conserv. 17 (3), 301–325.

Parkinson, R.W., DeLaune, R.D., White, J.R., 1994. Holocene sea-level rise and the fate of mangrove forest within the winder Caribbean region. J. Coast. Res. 10 (4), 1077–1086.

Perry, E., Paytan, A., Pedersen, B., Velazquez-Oliman, G., 2009. Groundwater geochemistry of the Yucatan Peninsula, Mexico: constraints on stratigraphy and hydrogeology. J. Hydrol. 367 (1), 27–40.

Pope, K.O., Duller, C.E., 1989. Satellite observations of ancient and modern water resources in the Yucatan Peninsula. In: Memoria, Simposio Latinoamericano sobre sensores remotos. Sociedad de Especialistas Latinoamericano en Percepción Remota and Instituto de Geografía, Universidad Nacional Autónoma de México, pp. 91–98.

Pope, K.O., Ocampo, A.C., Duller, C.E., 1993. Surficial geology of the Chicxulub impact crater, Yucatan, Mexico. Earth Moon Planet. 63 (2), 93–104.

Robbins, J.A., 1978. Geochemical and geophysical applications of radioactive lead. In: Nriagu, J.O. (Ed.), Biogeochemistry of Lead in the Environment. Elsevier, pp. 285–393.

Röllin, S., Sahli, H., Holzer, R., Astner, M., Burger, M., 2009. Pu and Np analysis of soil and sediment samples with ICP-MS. Appl. Radiat. Isot. 67 (5), 821–827.

Roman, C.T., Peck, J.A., Allen, J.R., King, J.W., Appleby, P.G., 1997. Accretion of a New England (USA) salt marsh in response to inlet migration, storms, and sea-level rise. Estuar. Coast. Shelf Sci. 45 (6), 717–727.

Ruiz-Fernández, A.C., Hillaire-Marcel, C., 2009. ^{210}Pb-derived ages for the reconstruction of terrestrial contaminant history into the Mexican Pacific coast: potential and limitations. Mar. Pollut. Bull. 59 (4), 134–145.

Ruiz-Fernández, A.C., Hillaire-Marcel, C., de Vernal, A., Machain-Castillo, M.L., Vásquez, L., Ghaleb, B., Páez-Osuna, F., 2009. Changes of coastal sedimentation in the Gulf of Tehuantepec, South Pacific Mexico, over the last 100 years from short-lived radionuclide measurements. Estuar. Coast. Shelf Sci. 82 (3), 525–536.

Ruiz-Fernández, A.C., Marrugo-Negrete, J.L., Paternina-Uribe, R., Pérez-Bernal, L.H., 2011. ^{210}Pb-derived sedimentation rates and Corg fluxes in soledad lagoon (Cispatá Lagoon System, NW Caribbean Coast of Colombia). Estuar. Coasts 34 (6), 1117–1128.

Ruiz-Fernández, A.C., Sanchez-Cabeza, J.A., de la Peña, J.L.S., Perez-Bernal, L.H., Cearreta, A., Flores-Verdugo, F., Machain-Castillo, M.L., Chamizo, E., García-Tenorio, R., Queralt, I., Dunbar, R., Mucciarone, D., Diaz-Asencio, M., 2016. Accretion rates in

coastal wetlands of the southeastern Gulf of California and their relationship with sea-level rise. The Holocene 0959683616632882.
Sanchez-Cabeza, J.A., Ruiz-Fernández, A.C., 2012. ^{210}Pb sediment radiochronology: an integrated formulation and classification of dating models. Geochim. Cosmochim. Acta 82, 183–200.
Sanchez-Cabeza, J.A., Ruiz-Fernández, A.C., Ontiveros-Cuadras, J.F., Bernal, L.H.P., Olid, C., 2014. Monte Carlo uncertainty calculation of ^{210}Pb sediment dating chronologies and accumulation rates of sediments and peat bogs. Quat. Geochronol. 23, 80–93.
Sanders, C.J., Smoak, J.M., Naidu, A.S., Araripe, D.R., Sanders, L.M., Patchineelam, S.R., 2010a. Mangrove forest sedimentation and its reference to sea level rise, Cananeia, Brazil. Environ. Earth Sci. 60 (6), 1291–1301.
Sanders, C.J., Smoak, J.M., Sanders, L.M., Naidu, A.S., Patchineelam, S.R., 2010b. Organic carbon accumulation in Brazilian mangal sediments. J. S. Am. Earth Sci. 30 (3), 189–192.
Sanders, C.J., Eyre, B.D., Santos, I.R., Machado, W., Luiz-Silva, W., Smoak, J.M., ... Silva-Filho, E., 2014. Elevated rates of organic carbon, nitrogen, and phosphorus accumulation in a highly impacted mangrove wetland. Geophys. Res. Lett. 41 (7), 2475–2480.
Sanders, C.J., Santos, I.R., Maher, D.T., Breithaupt, J.L., Smoak, J.M., Ketterer, M., Call, M., Sanders, L., Eyre, B.D., 2016. Examining $^{239+240}$Pu, ^{210}Pb and historical events to determine carbon, nitrogen and phosphorus burial in mangrove sediments of Moreton Bay, Australia. J. Environ. Radioact. 151, 623–629.
SEDESOL, 2016. Celestún: Datos Generales. http://www.microrregiones.gob.mx/zap/datGenerales.aspx?entra=zap&ent=31&mun=011 (consulted on 2016/05/29).
SEFOE, 2017. Celestún. Secretaría de Fomento Económico 2012–2018. http://www.sefoe.yucatan.gob.mx/secciones/ver/celestun (Consulted on 2017/07/11).
SMN (Servicio Mareográfico Nacional), 2017. http://www.mareografico.unam.mx/portal/index.php?page=Estaciones&id=8 (Consulted on 2017/06/28).
Smoak, J.M., Breithaupt, J.L., Smith, T.J., Sanders, C.J., 2013. Sediment accretion and organic carbon burial relative to sea-level rise and storm events in two mangrove forests in Everglades National Park. Catena 104, 58–66.
Stalker, J.C., Price, R.M., Rivera-Monroy, V.H., Herrera-Silveira, J., Morales, S., Benitez, J.A., Alonzo-Parra, D., 2014. Hydrologic dynamics of a subtropical estuary using geochemical tracers, Celestún, Yucatan, Mexico. Estuar. Coasts 37 (6), 1376–1387.
Stocker, T.F., Qin, D., Plattner, G.K., Tignor, M., Allen, S.K., Boschung, J., Nauels, A., Xia, Y., Bex, V., Midgley, P.M. (Eds.), 2013. Climate Change 2013: The Physical Science Basis. Contribution of Working Group I to the Fifth Assessment Report of the Intergovernmental Panel on Climate Change. Cambridge University Press, Cambridge, United Kingdom, and New York, NY, USA.
Tateda, Y., Nhan, D.D., Wattayakorn, G., Toriumi, H., 2005. Preliminary evaluation of organic carbon sedimentation rates in Asian mangrove coastal ecosystems estimated by ^{210}Pb chronology. Radioprotection 40 (S1), S527–S532.
Twilley, R.R., Chen, R.H., Hargis, T., 1992. Carbon sinks in mangroves and their implications to carbon budget of tropical coastal ecosystems. Water Air Soil Pollut. 64 (1–2), 265–288.
UNESCO, 2016. Biosphere Reserves – Learning Sites for Sustainable Development. http://www.unesco.org/new/en/natural-sciences/environment/ecological-sciences/biosphere-reserves/ (consulted on 2016/05/29).
Wedepohl, K.H., 1971. Environmental influences on the chemical composition of shales and clays. Phys. Chem. Earth 8, 307–333.
Wilson, E.M., 1980. Physical Geography of the Yucatan Peninsula. Yucatan: A World Apart. University of Alabama Press, Tuscaloosa (5e40).
Wu, X., Heflin, M.B., Schotman, H., Vermeersen, B.L., Dong, D., Gross, R.S., Ivins, E.R., Moore, A.W., Owen, S.E., 2010. Simultaneous estimation of global present-day water transport and glacial isostatic adjustment. Nat. Geosci. 3 (9), 642–646.
Zavala-Hidalgo, J., de Buen Kalman, R., Romero-Centeno, R., Maguey, F.H., 2010. Tendencias del nivel del mar en las costas mexicanas. In: Botello, A.V., Villanueva-Fragoso, S., Gutiérrez, J., Rojas Galaviz, J.L. (Eds.), Vulnerabilidad de las zonas costeras mexicanas ante el cambio climático. SyG Editores, Gobierno del Estado de Tabasco, Semarnat-INE, UNAM-ICMyL, Universidad Autónoma de Campeche, México, pp. 249–267.
Zimmerman, A.R., Canuel, E.A., 2000. A geochemical record of eutrophication and anoxia in Chesapeake Bay sediments: anthropogenic influence on organic matter composition. Mar. Chem. 69 (1), 117–137.